Paper II

J Neurosurg 104:118–128, 2006

Antitumor efficacy improved by local delivery of species-specific endostatin

Peter C. Huszthy, M.Sc., Christian Brekken, Ph.D., Tina B. Pedersen, Frits Thorsen, Ph.D., Per Øystein Sakariassen, M.Sc., Kai Ove Skaftnesmo, M.Sc., Olav Haraldseth, M.D., Ph.D., Per Eystein Lønning, M.D., Ph.D., Rolf Bjerkvig, Ph.D., and Per Øyvind Enger, M.D., Ph.D.

Gene Therapy Program, Department of Oncology and Medical Physics, Haukeland University Hospital, Bergen, Norway; Department of Circulation and Medical Imaging, Norwegian University of Science and Technology, Trondheim, Norway; NorLux Neuro-Oncology, Department of Biomedicine, University of Bergen, Norway; NorLux Neuro-Oncology, Centre Recherché Public Santé, Luxembourg; and Department of Neurosurgery, Haukeland University Hospital, Bergen, Norway

Object. Conflicting results have been reported concerning the antitumor efficacy of the angiogenesis inhibitor endostatin. This may be due to differences in the biological distribution of endostatin between studies or to the varying biological efficacies of the different protein forms that were examined. To address this issue, the authors used a local delivery approach in which each tumor cell secreted endostatin, providing uniform endostatin levels throughout the tumors. This allowed a direct assessment of the biological efficacy of soluble endostatin in vivo.

Methods. The authors genetically engineered BT4C gliosarcoma cells so that they would stably express and secrete either the human or murine form of endostatin. Endostatin-producing cells or mock-infected cells were implanted intracerebrally in syngeneic BD-IX rats. The antitumor efficacy of endostatin was evaluated on the basis of survival data and tumor volume comparisons. In addition, microvascular parameters were assessed.

The authors confirmed the continuous release of endostatin by the BT4C cells. A magnetic resonance imaging–assisted comparison of tumor volumes revealed that local production of murine endostatin significantly inhibited tumor growth. Notably, 40% of the animals in this treatment group experienced long-term survival without histologically verifiable tumors 7 months after cell implantation. After local treatment with murine endostatin, tumor blood plasma volumes were reduced by 71%, microvessel density counts by 84%, and vascular area fractions by 75%. In contrast, human endostatin did not inhibit tumor growth significantly in this model. Centrally located regions of necrosis were present in tumors secreting both the human and the murine species-specific form of endostatin.

Conclusions. The results suggest that endostatin inhibits tumor angiogenesis in vivo in a species-specific manner.

Key Words • endostatin • local drug delivery • brain neoplasm • species-specific form • angiogenesis

Glioblastoma multiforme differs from low-grade gliomas by its histological evidence of angiogenesis and necrosis.[27] Endothelial proliferation and the assembly of a new vascular network allow for rapid tumor mass expansion and coincide with a marked worsening of prognosis. Thus, the onset of angiogenesis is a key event during brain tumor progression. Single-cell infiltration into brain tissue makes complete surgical removal impossible, with tumor recurrence at the resection site being the major cause of GBM-associated deaths.[9] Therefore, the application of angiogenesis inhibitors as adjuvant treatment to impede tumor regrowth seems well founded.[32] The principle of exploiting angiogenesis inhibitors for cancer therapy was proposed more than 30 years ago,[20] and as of today several inhibitors have been examined in clinical trials.[18]

Endostatin was initially purified from a murine hemangiothelioma cell line.[35] It proved to be a C-terminal fragment of collagen XVIII, an extracellular matrix component that occurs in blood vessel walls and in the basement membranes of the liver, kidney, and lung.[34] Endostatin may be cleaved from collagen XVIII by several proteolytic enzymes,[17] many of which are expressed during tumor cell migration and metastasis.[28]

Endostatin inhibits the proliferation, migration, and survival of endothelial cells.[10–12,15,41,46] On the molecular level, blockage of signaling through the vascular endothelial growth factor receptor,[21,24] suppression of Wnt-signaling by ß-catenin destabilization,[13] inhibition of metalloproteinas-

Abbreviations used in this paper: cDNA = complementary DNA; CSF = cerebrospinal fluid; EGFP = enhanced green fluorescent protein; ELISA = enzyme-linked immnosorbent assay; FITC/TRITC= fluorescein isothiocyanate/tetramethylrhodamine isothiocyanate; GBM = glioblastoma multiforme; MR = magnetic resonance; ROI = region of interest; SEM = standard error of the mean; TBS =Tris-buffered saline.

es,[25] and downregulation of c-*myc*[40] and cyclin D1[22] have been proposed as downstream effects of endostatin's interaction with its target molecules. Importantly, the processes acted on by endostatin are exclusive to new vessel formation; therefore, quiescent vasculature is not affected.[2,13,42,43]

The antitumor potency of recombinant endostatin was a subject of controversy during the last decade. Initial reports demonstrated regression of preestablished subcutaneous tumors in mice, leaving microscopic, dormant nodules that failed to regrow after repeated therapy.[5,6,35] Although most subsequent studies have confirmed endostatin's inhibitory effect on tumor growth, eradication of established tumors and sustained survival of affected animals has not been reproduced.[3,4,38] More contradictory results have been reported by others, who found no effect on tumor growth or metastatic spread, even when high systemic concentrations were obtained.[14,36]

Notably, high systemic levels of an angiogenesis inhibitor may not necessarily ensure sufficient concentration at the tumor site. Furthermore, both precipitated and soluble forms of human and murine endostatin have been used throughout these studies[42] without a systematic comparison of their therapeutic efficacies. Therefore, both the variations in endostatin biodistribution and the differences in biological efficacy of the different protein forms may have contributed to conflicting data regarding endostatin's antitumor efficacy.

To distinguish between these parameters, we used genetically modified tumor cells that stably expressed and released endostatin. This provided continuous local delivery, thereby eliminating variations in biological distribution as a source of error, allowing us to assess the in vivo biological efficacy of endostatin in a more direct manner. Our findings demonstrate that tumors that provide local production of murine endostatin inhibit angiogenesis, leading to suppressed tumor growth when compared with both mock-infected tumors and tumors that overexpress human endostatin. We suggest that the unequivocal results obtained in previous studies may be attributed to both inadequate biological distribution and to the differences in activity between the endostatin species-specific forms.

Materials and Methods

Cell Lines and Culture Conditions

The BT4C rat gliosarcoma cells[31] were grown in Dulbecco modified Eagle medium supplied with 10% heat-inactivated newborn calf serum, four times the prescribed concentration of nonessential amino acids, L-glutamine, penicillin (100 IU/ml), and streptomycin (100 μg/ml). Phoenix Eco packaging cells (SD 3444; American Type Culture Collection, Manassas, VA) were cultured in the same medium, except that the newborn calf serum was replaced with heat-inactivated fetal calf serum. The cells were kept in a 37°C humidified incubator with an atmosphere containing 5% CO_2.

Vector Construction

The pCEP/Pu-AC7 expression vector[29] contained either the human or the murine endostatin cDNA fused to the secretion signal peptide sequence of the BM-40 protein. The expression cassettes were released from pCEP/Pu-AC7 by endonuclease treatment with *Hpa*I and *Hind*III, and subcloned into the pLNCX retroviral vector containing the neomycin resistance gene (Clontech Laboratories, Inc., Palo Alto, CA) to yield recombinant vectors containing cDNA for murine endostatin (pLNCX-mENDO) or human endostatin (pLNCX-hENDO). The absence of mutations in both constructs was verified by polymerase chain reaction sequencing and sequence comparison analysis by using appropriate software (Edit View program, version 1.0.1; Applied Biosystems, Foster City, CA) with the BLASTn search tool. The pLEGFP-N1 expression vector (Clontech Laboratories, Inc.) was used to generate retroviruses containing the EGFP cDNA, to be used as positive controls for the infection and selection process.

Generation of Recombinant Retroviral Particles

The pLNCX-mENDO, pLNCX-hENDO, and pLEGFP-N1 expression vectors and the pLNCX expression vector without an insert were transfected into the Phoenix Ecotrophic packaging cells by standard calcium phosphate DNA precipitation.[1] Retrovirus-containing conditioned medium was harvested from the packaging cells every 12 hours beginning 48 hours posttransfection. The medium was supplemented with hexadimethrine bromide (Polybrene; Sigma, St. Louis, MO) to 4 μg/ml and added immediately onto subconfluent BT4C cells through a 0.45-μm polyether sulfon syringe filter (Pall Gelman Laboratory, Ann Arbor, MI). No replication-competent retroviruses were detected in the supernatants when we performed serial infections of new batches of BT4C cells.

Retroviral Transduction

Forty-eight hours postinfection, the BT4C cells were selected for the neomycin resistance gene contained in the expression vector by using 1.3 mg/ml G418 (Sigma, St. Louis, MO). Selective pressure was maintained during further culturing. After selection, individual resistant clones were isolated using sterile cloning rings and transferred to individual wells in 24-well plates. Cells expressing murine endostatin were designated BT4C mENDO, those expressing human endostatin were designated BT4C hENDO, and mock infectants were designated BT4C mock. Green fluorescence protein expression in the EGFP–positive BT4C cells was observed with the aid of a Leica confocal laser microscope with fluorescein isothiocyanate/tetramethylrhodamine isothiocyanate filter settings (TCS-NT; Leica Microsystems Heidelberg GmbH, Heidelberg, Germany).

Assessment of Endostatin Production

To verify endostatin protein secretion from the selected cell clones, conditioned culture media were collected and evaluated using Western blot analysis. Confluent monolayers of cells in 75-cm^3 flasks were overlaid with 6 ml OptiMEM serum-free medium (Life Technologies, Gaithersburg, MD) and incubated for 24 hours. Conditioned medium from BT4C mock cells was prepared the same way and used as a negative control. Twenty-microliter samples of the media were run under reducing conditions on 12% polyacrylamide gels followed by transfer to 0.2-μm Protran nitrocellulose membranes (Schleicher & Schuell, Dassel, Germany). For detection of human endostatin, the membranes were probed with rabbit anti–human endostatin antiserum or with purified rabbit anti–human endostatin antibodies (Chemicon, Inc., Temecula, CA) at a 1:1000 or 1:100 dilution, respectively. Murine endostatin was detected using purified rabbit anti–mouse endostatin antibodies (Chemicon, Inc.) at a 1:100 dilution. Positive bands for endostatin were visualized using chromogenic substrates catalyzed by alkaline phosphatase– or horseradish peroxidase–conjugated secondary antibodies (Dako Cytomation, Glostrup, Denmark) at a 1:1000 dilution. To quantify the amount of released endostatin, conditioned media samples were collected after a 24-hour incubation period and analyzed using sandwich ELISA (enzyme immunoassay kits) (CytElisa; Nordic Biosite AB, Täby, Sweden) following the manufacturer's instructions. The kits contained specific antibodies directed against the human or murine species-specific form of endostatin. To quantify endostatin secretion in vivo, CSF samples obtained from animals implanted with cells and control animals were analyzed similarly by Western blot analysis and sandwich ELISA. In addition, the concentration of endostatin in the conditioned culture medium from an explanted tumor spread out in a monolayer cell culture was quantified after 48 hours of incubation by using a competitive ELISA kit (Accucyte; Nordic Biosite AB).

Tumor Inoculation

Forty-five male and female BDIX rats, each weighing between 50 and 100 g, were maintained on a standard pellet diet, given unlimited access to water, and caged at constant temperature and humidity.

Anesthesia was induced in the rats by a subcutaneous injection of midazolam (0.2 g/100 g), fentanyl citrate (0.0126 g/100 g), and fluanizone (0.4 g/100 g) before the animals were mounted in a small animal stereotactic frame (model 900; David Kopf Instruments, Tujunga, CA). Following a midsagittal incision, a bur hole was prepared 1 mm posterior to the bregma and 3 mm to the right of the midline suture. A 5-μl suspension containing either BT4C mENDO cells (15 rats), BT4C hENDO cells (15 rats), or BT4C mock cells (15 rats) was injected, with the aid of a 10-μl Hamilton syringe connected to a micropump, to a depth of 2.5 mm from the dura mater. For all animals, a total of 40,000 cells were implanted. The animals were observed daily and were killed by an overdose of CO_2 when neurological symptoms occurred. The experiments were terminated 7 months postimplantation, at which time all the remaining animals were killed. All experiments were approved by the Norwegian Animal Research Authority and were in accordance with the Animal (Scientific Procedures) Act of 1986.

Magnetic Resonance Imaging and Analysis of Vascular Parameters

The animals were evaluated for tumor growth and the presence of necrosis 3 weeks postimplantation by using an MR imaging system (Magnetom Vision Plus 1.5-tesla unit; Siemens, Erlangen, Germany) and a small loop finger coil as previously described.[45] After they had been anesthesized, the rats were fixed in a polystyrene immobilizing tube. Coronal T_1-weighted sequences (TR 400 msec, TE 14 msec, slice thickness 2 mm, and distance between the centers of slices 2 mm in all 13 coronal slices covering the forebrain) were obtained before and after a subcutaneous injection of contrast agent (1 ml Gd, 0.5 mmol/ml), and coronal T_2-weighted sequences (TR 4000 msec, TE 96 msec, slice thickness 2 mm, distance between centers of slices 2 mm, in a total of 19 coronal slices covering the forebrain) were also obtained.

To assess microvascular function and tumor volumes, the rats underwent dynamic contrast-enhanced T_1-weighted MR imaging at 2.35 teslas by using another MR imaging unit (Bruker Biospec Avance DBX-100; Bruker BioSpin MRI GmbH, Ettlingen, Germany). Anesthesia was induced in the animals and continuously maintained by the administration of 1 to 2% isoflurane in 70/30% N_2/O_2 through a face mask. The rats were placed supine on a cradle filled with circulating fluorocarbons at 37 to 38°C. A polyethylene catheter was inserted into the right femoral vein for intravenous injection of contrast agent. The following key parameters for the dynamic contrast-enhanced sequence were used: 10 axial slices, slice thickness 3 mm, field of view 3.5 cm, matrix size 64 × 64, TR 82.5 msec, TE 5 msec, total acquisition time approximately 18 minutes. Contrast agent was injected as a short bolus after acquisition of four baseline images. Signal intensity was converted to a Gd concentration by using pre–contrast agent administration T_1 values from T_1 maps based on spin echo images (TRs 100, 300, 500, 1500, and 2000 msec; TE 8.8 msec) with a geometry identical to that used for the dynamic imaging sequence.

The microcirculatory transport of tracer in the tumor tissue was characterized by the following tracer kinetic constant parameters: D_0 (in mM), proportional to the blood plasma volume fraction; D_1 (in mM/minute), proportional to the transfer constant of tracer from blood plasma to the extravascular compartment multiplied by the leakage space volume fraction; and K_2 (1/minute), proportional to the ratio between the transfer constant of the tracer from the extravascular compartment to blood plasma and the leakage space volume fraction.[44] The tracer kinetic constants D_0, D_1, and K_2 were obtained by curve fitting according to the method proposed by Su and colleagues.[44] An entire tumor ROI (> 100 pixels) was selected from the middle slice at the time point of peak intensity (2–3 minutes after contrast agent administration), and parametric maps were obtained. The values are reported as the mean numbers of pixels in the tumor ROI. When no tumor was apparent, an ROI of 300 pixels was placed at the site of tumor cell implantation.

Immunostaining and Assessment of Microvessel Density and Area Fractions

Formalin-fixed, paraffin-embedded tissue sections were placed in a xylene bath (two times for 3 minutes each), followed by baths in absolute ethanol (two times for 3 minutes each), 96% ethanol (two times for 3 minutes each), and distilled water (30 seconds) for removal of the paraffin and rehydration. The following primary antibodies were used, diluted in TBS: polyclonal rabbit anti–human von Willebrand factor (Dako Cytomation, 1:500), rabbit anti–human endostatin (Chemicon, Inc., Temecula, CA, 1:400), or rabbit anti–murine endostatin (Chemicon, Inc., 1:100). The tissue sections were stained using the EnVision+ system (Dako Cytomation), using horseradish peroxidase-conjugated secondary antibodies and 3′3-diaminobenzidine for signal development. The manufacturer's protocol was followed. Routine Harris H & E counterstaining was performed to visualize the tissue structure and the morphological characteristics of the nucleus.

Sections immunostained for von Willebrand factor were inspected for areas of high microvessel density at 40 magnification. In each tumor, 25 regions (five visual fields in five areas) were selected for a closer analysis at 400 magnification. For image acquisition, the observers set a threshold to distinguish vascular elements from surrounding tissue, which were then assessed using a morphometry software package (LUCIA G software; Laboratory Imaging Ltd., Prague, Czech Republic).

Statistical Analysis

The survival time of the animals, microvessel densities, and vascular area fractions were analyzed using GraphPad Prism statistical software (GraphPad Software, San Diego, CA). For dynamic contrast-enhanced MR images, data plotting and statistical analysis were performed using the SPSS software package (version 10.1; SPSS Inc., Chicago, IL). Spearman rank correlation tests were applied at a significance level of 0.01. For a comparison of tumor volumes, the differences among the three groups were analyzed using the Kruskal–Wallis test for independent multiple variables. Thereafter, tumor volumes within in each treatment group were compared with those in the control group by applying the Mann–Whitney test for two-group comparisons.

Results

Endostatin Expression in Retrovirally Transduced BT4C Cells

To generate recombinant retroviruses carrying human or murine endostatin cDNA, the respective sequences were subcloned into the pLNCX retroviral expression vector. The secretion signal peptide sequences were fused to the endostatin sequences to ensure secretion of the protein from the transduced cells. Production of infectious particles was conducted as described earlier.

The expression cassettes of the retroviral vectors are shown in Fig. 1B. To evaluate the efficiency of the gene transfer, the entire transduction and selection procedure was performed in pairs when a parallel batch of cells was infected with *EGFP*-encoding retroviruses. Following antibiotic selection, nearly 100% transgene expression was obtained, as detected by fluorescence microscopy (Fig. 1C). Endostatin production and release was validated in vitro, in vivo, and ex vivo by performing Western blot analyses of tumor cell–conditioned media and CSF samples. Murine and human endostatin each appeared as a clear, single band of 22 kD on the Western blots (Fig. 1D). Endostatin was detected in media samples conditioned by BT4C cells after antibiot-

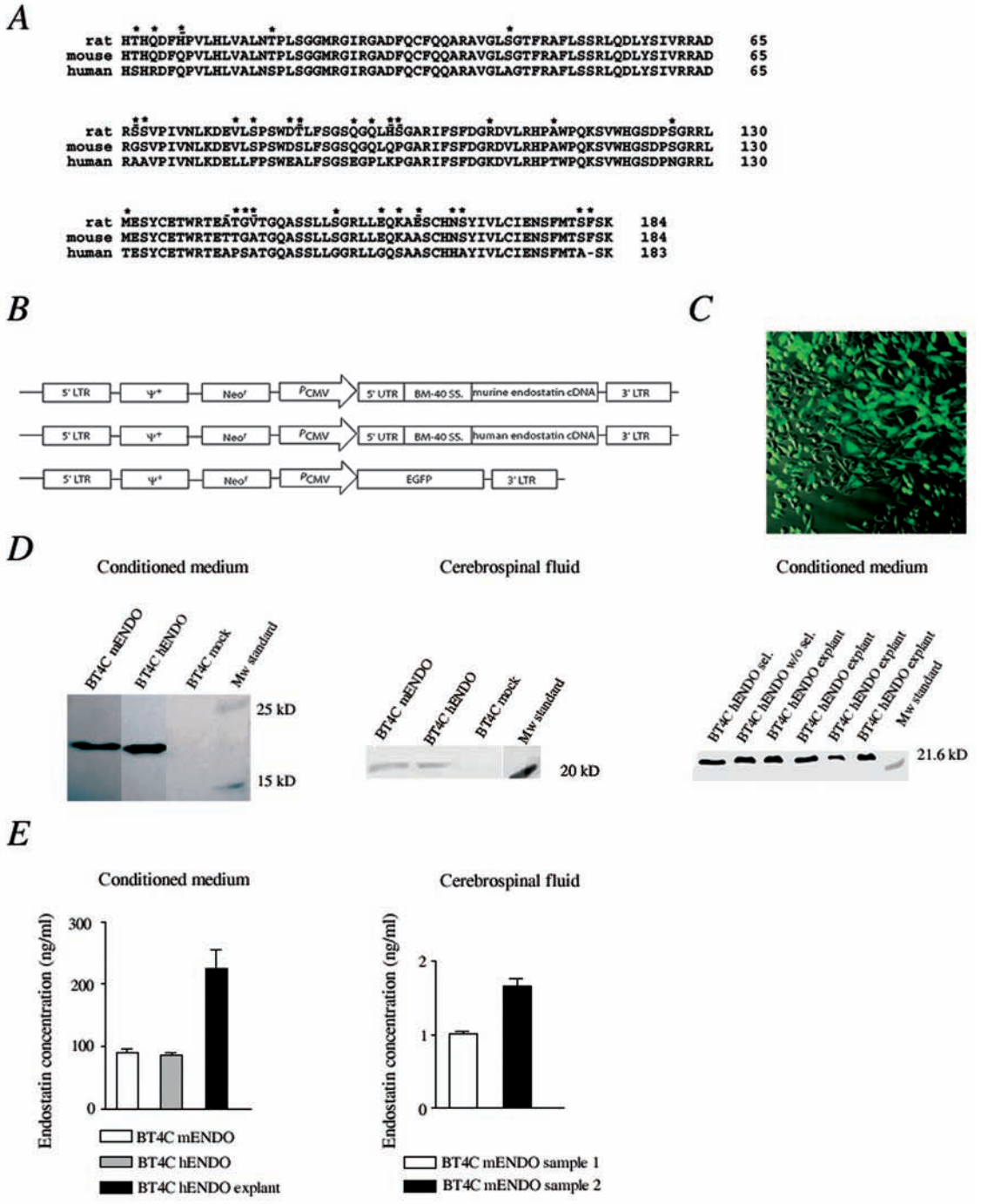

FIG. 1. A: Protein sequence alignment among the rat, mouse, and human forms of endostatin. *Asterisks* mark the amino acid substitutions between rat and human sequences and *lines* mark the substitutions between rat and mouse sequences. B: Schematic depiction of the retroviral expression cassettes containing murine and human endostatin or EGFP cDNA sequences. C: Photomicrograph showing EGFP-expressing BT4C cells after retroviral infection. Nearly 100% of the cells display a positive signal for EGFP after antibiotic selection. Original magnification × 200. D: Western blot analysis of endostatin production and release from the retrovirally infected BT4C cells in vitro (tumor cell–conditioned media, *left*), in vivo (CSF, *center*) and ex vivo (tumor explant–conditioned media, *right*). E: Bar graphs showing endostatin levels measured by ELISA in tumor cell–conditioned culture media (*left*) and CSF samples (*right*). No endostatin was detected in media conditioned by BT4C mock-infected cells or in CSF of control animals. BM-40 SS = secretion signal peptide sequence of the BM-40/osteonectin/SPARC protein; BT4C hENDO = BT4C cell clone infected with retroviruses carrying the human endostatin cDNA; BT4C mENDO = BT4C cell clone infected with retroviruses carrying the murine endostatin cDNA; BT4C mock = BT4C cell clone infected with empty retroviruses; LTR = long terminal repeats; Neo^r = neomycine resistance gene; P_{CMV} = human cytomegalovirus immediate early promoter; 5′UTR = 5′ untranslated terminal repeats; Ψ^+ = extended viral packaging signal.

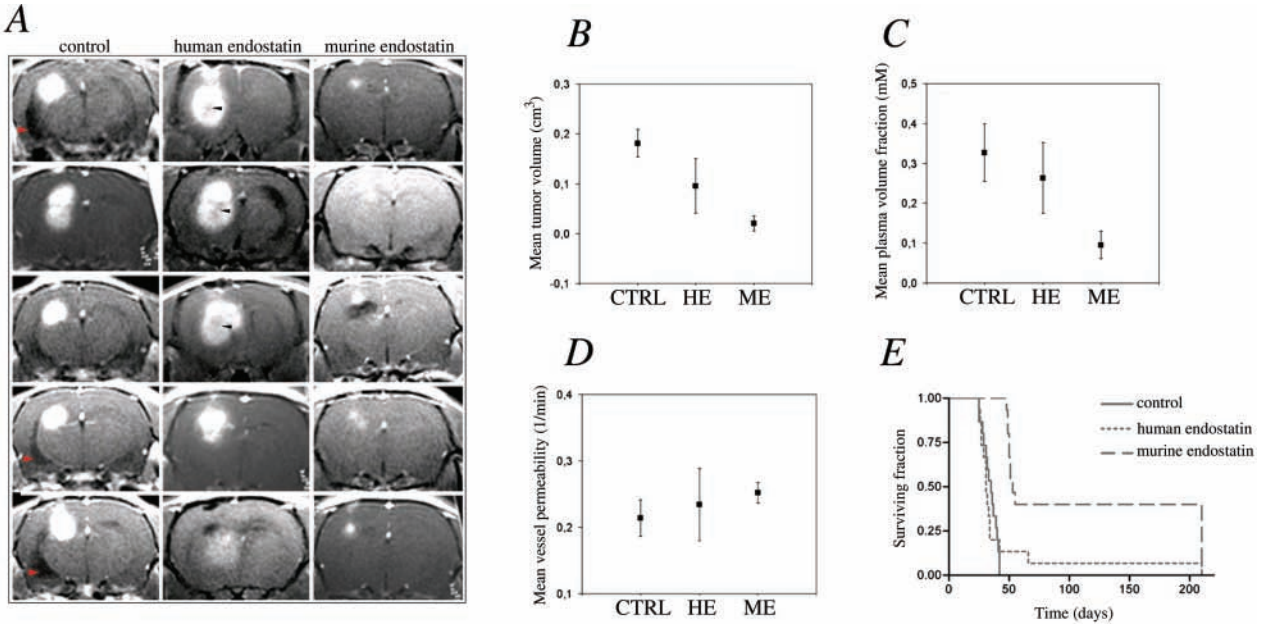

FIG. 2. A: Several Gd-enhanced T_1-weighted MR images obtained 3 weeks after implantation of tumor cells. All the tumors demonstrate strong contrast enhancement. In several animals, tumor growth is accompanied by obstructive hydrocephalus with entrapment of CSF in the lateral ventricles (*red arrowheads*). Within the endostatin-treated tumors, central low-signal areas indicating necrosis are present (*black arrowheads*). B–D: Graphs showing assessments of mean tumor volumes (B; for each group, five animals each); mean plasma volume fractions (D_0) calculated from functional MR imaging data (C; for each group, five animals each); and mean microvessel permeability values (K_2) calculated from functional MR imaging data (D; for each group, five animals in each group). E: Kaplan–Meier survival curve for the three groups (15 animals in each group). CTRL = control group; HE = human endostatin–treated group; ME = murine endostatin–treated group.

ic selection (Fig. 1D *left*). In addition, when the cells were cultured without selective antibiotic pressure for 10 weeks (similar to the in vivo setting), endostatin secretion was maintained at similar levels (Fig. 1D *right*). Lower levels of endostatin were detected in the CSF samples than in the conditioned media (Fig. 1D *center*). A yield of at least 40 μl CSF was necessary to detect endostatin in this setting.

For further verification, some of the endostatin-producing tumors were dissected out, minced, and plated in selective medium. We did not observe substantial cell death, suggesting that the neomycin resistance conferred by the vector was not inactivated in vivo. Endostatin production and release from the explanted tumor cells was detected at levels similar to that before implantation (Fig. 1D *right*).

Assessment of Endostatin Levels In Vitro and In Vivo

We quantified the concentration of endostatin present in the conditioned media and CSF samples by performing ELISAs. The BT4C hENDO cells released 86.0 ± 4.9 ng/ml (mean ± SEM) human endostatin, whereas the BT4C mENDO cells released 91.2 ± 6.1 ng/ml murine endostatin during a 24-hour period in culture (Fig. 1E). In all cases, the levels of endostatin in the conditioned media from BT4C cells infected by empty vectors were below the standard curve range.

The concentrations of murine endostatin in two different CSF samples were 1.01 ± 0.03 and 1.67 ± 0.11 ng/ml (Fig. 1E right, three measurements for each sample). The concentration of human endostatin in the culture medium conditioned by a tumor explant in monolayer was found to be 225.5 ± 30.3 ng/ml following 48 hours of incubation (Fig. 1E *left*).

Tumor Progression

To evaluate tumor growth, all animals were examined by performing MR imaging 3 weeks after cell implantation. The tumors appeared as expansive, strongly contrast-enhancing lesions on T_1-weighted sequences following injections of Gd (Fig. 2A). In several animals, the presence of the tumor was accompanied by obstructive hydrocephalus with entrapment of CSF in the lateral ventricles (Fig. 2A, *red arrowheads*). The presence of tumor was confirmed in all the control animals. In the group of rats treated with human endostatin, all but two rats had a visible lesion at the time of MR imaging. In one of these a brain tumor developed at a later stage, leading to the death of the animal. The other rat did not display any symptom during the time course of the experiment, and no visible tumor was recorded on histological examination. In the group of rats implanted with BT4C cells secreting murine endostatin, no visible tumors were detected by MR imaging in six of the animals. All these animals remained free from symptoms during an observation period that lasted 7 months. After the animals had been killed, their brains did not appear to harbor any tumor on macroscopic inspection or histological examination. The human endostatin–secreting tumors varied in size, but were not significantly smaller than those in the control group. Several of these tumors displayed a low signal intensity ar-

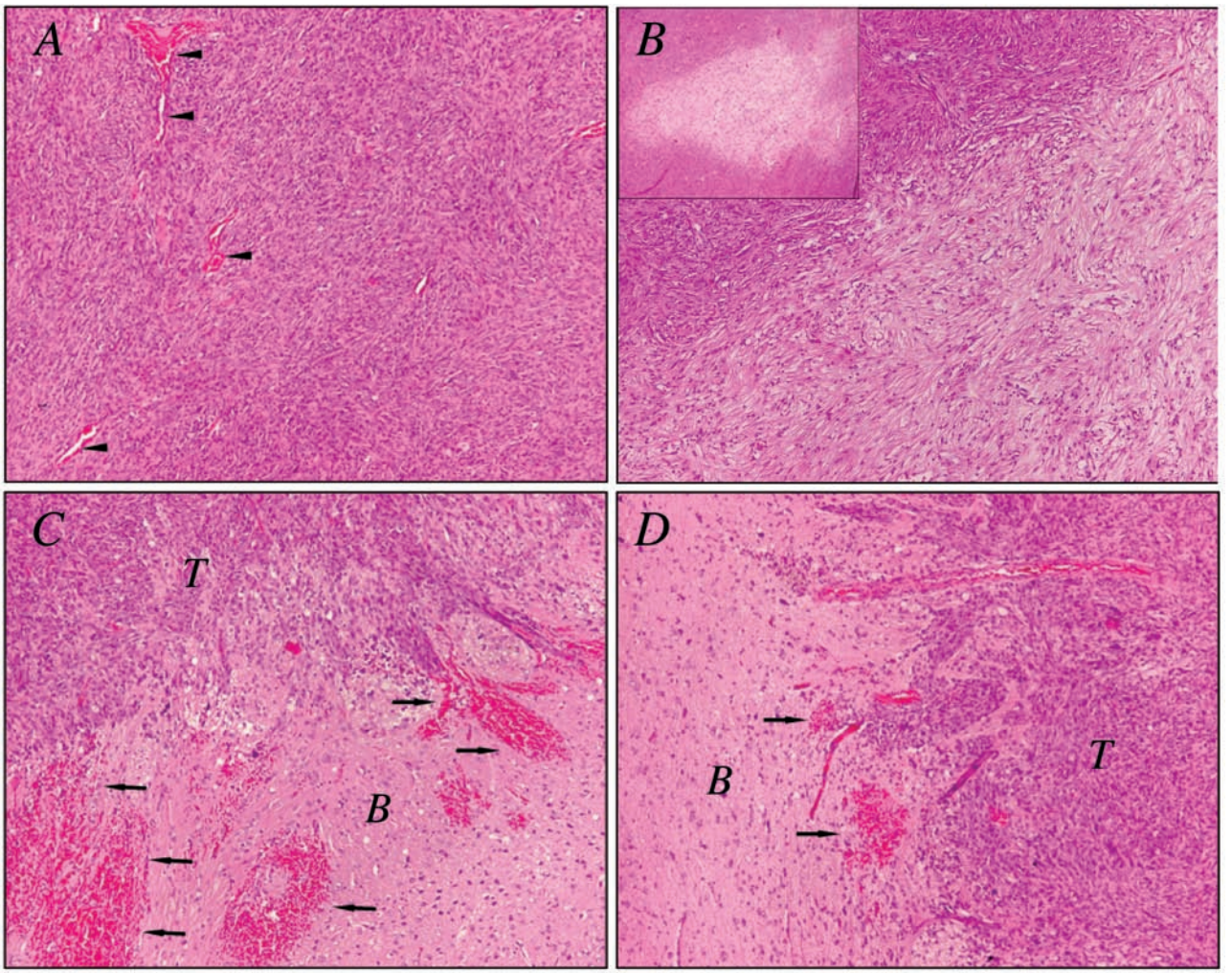

FIG. 3. Photomicrographs showing tumor sections. A: Tissue with markedly dilated blood vessels (*arrowheads*) located centrally in a control tumor. Such dilated vessels were absent in treated tumors. B: Central necrosis within an endostatin-treated tumor. Inset shows an overview of the necrotic area in the central tumor region. C and D: Leakage of blood from the tumor vasculature into the extravascular space (marked by *arrows*) was seen in both endostatin-treated (C) and control (D) tumors. *B* = brain tissue; *T* = tumor. H & E, original magnifications × 100 (A– D) and × 40 (*inset*).

ea centrally, however, suggesting the presence of necroses. This was later verified by histological examination.

Tumor Volumes

Tumor volume estimates were obtained by manual segmentation of MR imaging data that were corrected for interslice distances. The mean (± SEM) tumor volumes were 0.021 ± 0.015 cm^3 for five animals in the murine endostatin–treated group, 0.095 ± 0.055 cm^3 for five animals in the human endostatin–treated group, and 0.181 ± 0.028 cm^3 for four animals in the control group, as estimated from a review of MR images obtained 3 weeks postimplantation (Fig. 2B). Differences among the three groups were of statistical significance ($p = 0.029$, Kruskal–Wallis test). A paired comparison revealed a significant difference in tumor reduction between the murine endostatin–secreting tumors and control lesions ($p = 0.016$), whereas the difference in tumor volume between human endostatin–secreting tumors and control lesions was not significant ($p = 0.19$).

Functional Characterization of Endostatin Treatment on Glioma Vasculature

The D_0, proportional to the blood plasma volume fraction, was significantly lower in the murine endostatin–treated group (0.095 ± 0.034 mM [mean ± SEM]), but not in the human endostatin-treated group (0.263 ± 0.088 mM), when compared with that of the control group (0.327 ± 0.073 mM; Fig. 2C). Microvessel permeability, K_2, did not differ significantly among the groups (means ± SEMs: 0.252 ± 0.042/minute in the murine endostatin–treated group, 0.234 ± 0.04/minute in the human endostatin–treated group, and 0.214 ± 0.017/minute in the control group; Fig. 2D).

Survival Data

The duration of survival for each animal was defined as the time from tumor cell implantation to the occurrence of symptoms related to tumor growth, at which point the animal was killed. Animals treated with murine endostatin

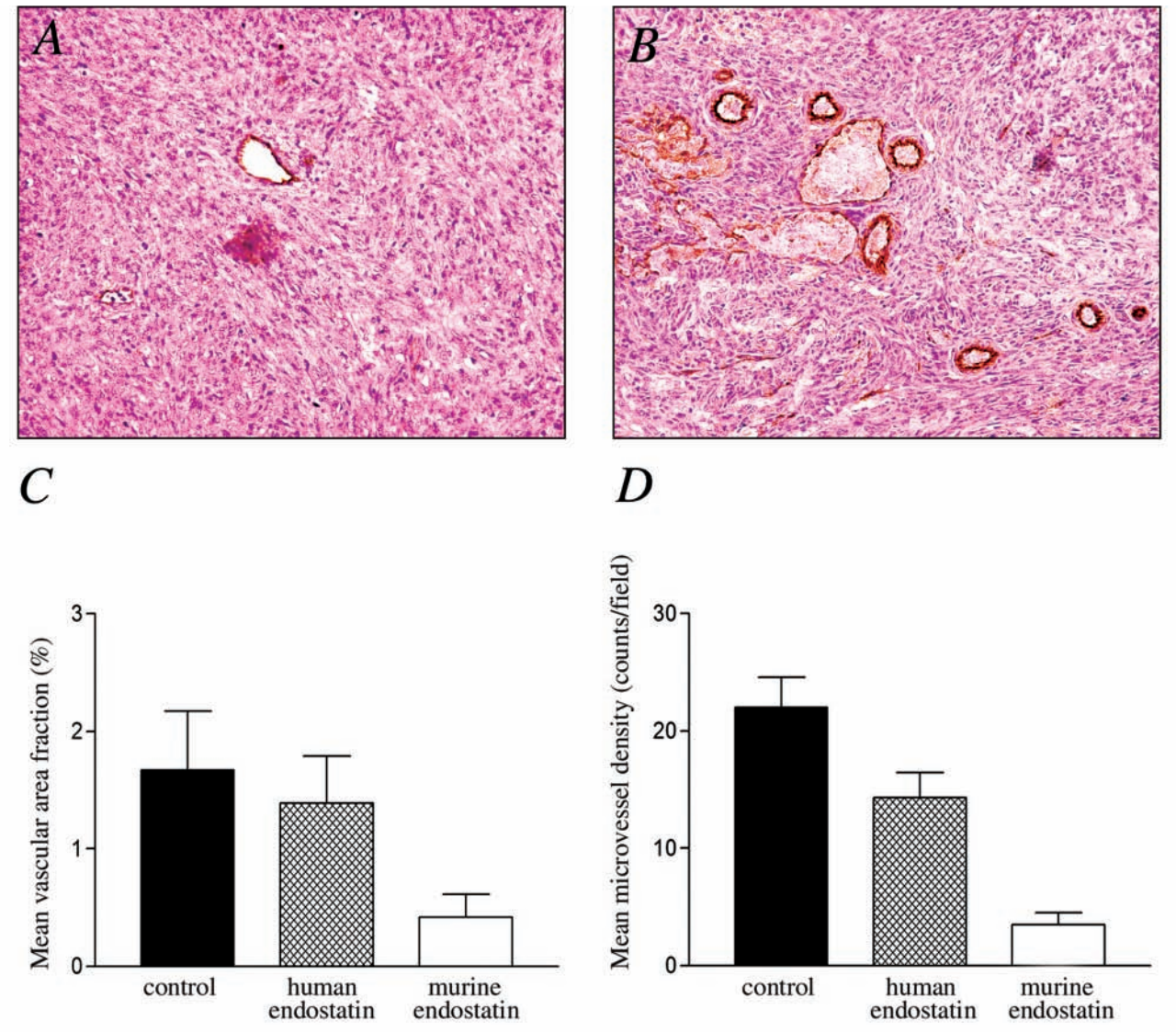

FIG. 4. A and B: Photomicrographs showing representative tumor sections immunostained against von Willebrand factor in murine endostatin–treated (A) and control (B) tumors. Original magnification × 200. C and D: Bar graphs demonstrating mean vascular area fractions and microvessel density counts quantified from the immunostained sections.

lived significantly longer than animals in the other two groups ($p < 0.0001$), with a mean (± SEM) survival of 114.4 ± 20.9 days.

Notably, 40% of the animals in the murine endostatin treatment group remained free from tumor during the entire observation period. In the control group, the mean (± SEM) survival was 34.3 ± 1.5 days, whereas in the group of rats treated with human endostatin it was 45.2 ± 12.1 days. Although the latter group did not have a significantly longer mean survival time, no tumor developed in one animal and in another animal, the survival time was prolonged (72 days) despite the appearance of a tumor.

Histological Characteristics of the Tumors

Rat brains from the treatment groups and the control group were sectioned and stained with H & E. In the control lesions (BT4C mock), the cells had a pleomorphic appearance with atypical nuclei and numerous mitotic figures. The angioarchitecture in the tumor bulk was deranged, with irregular, markedly dilated vessels and several sites of endothelial cell proliferation (Fig. 3A). In tumors that released human or murine endostatin, large necrotic areas were present in the central regions (Fig. 3B). Necrotic regions were not seen in control lesions, which appeared homogeneous and hypercellular. In specimens from both treated and control groups, abnormal vessels were observed at the host–tumor interface, with leakage of blood into the extravascular space, indicating a disrupted blood–brain barrier (Fig. 3C and D).

Microvessel Density and Vascular Area Fraction

Tumor specimens from animals in the treatment and control groups were immunostained for the endothelial cell marker von Willebrand factor, which allowed for the assessment of microvessel density and vascular area fractions

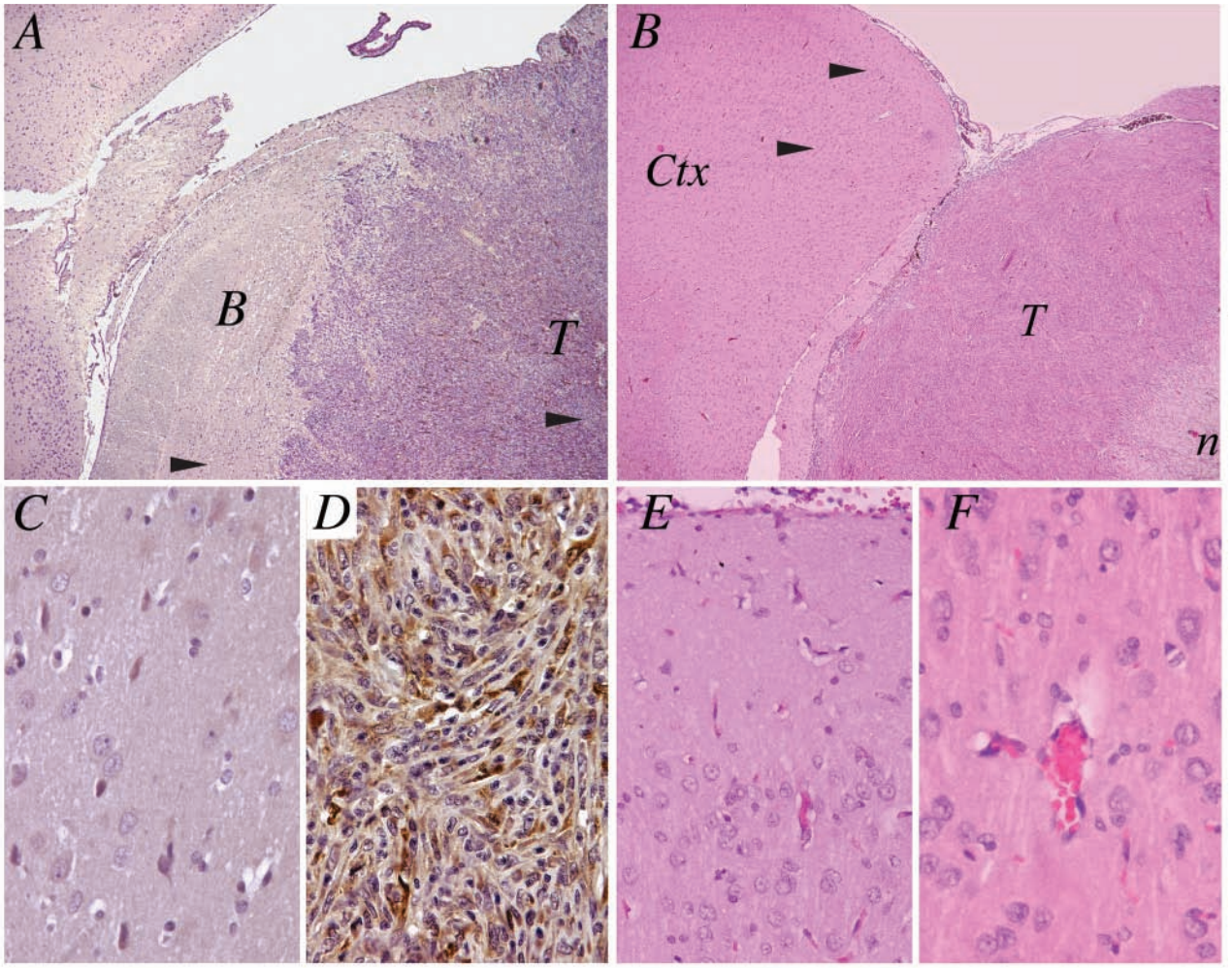

FIG. 5. Photomicrographs. A: Overview of an endostatin-secreting tumor immunostained for human endostatin. Endostatin expression is seen throughout the tumor tissue. *Arrowheads* point to areas selected for higher magnification in C and D. B: Overview of tissue from an endostatin-secreting tumor with large central necrosis. To the left is the surrounding host brain tissue. *Arrowheads* point to cortical areas selected for higher magnification in panels E and F. C: Area of brain tissue selected from panel A. The brain tissue adjacent to the tumor does not stain for endostatin. D: Central area of tumor tissue selected from panel A. The glioma tissue exhibits strong positive staining for endostatin localized to the cytoplasm of the BT4C hENDO cells. E: Area of tissue selected from panel B showing the frontal cortex area with the normal morphological characteristics of the cortical layer. Several microvessels are present, suggesting good perfusion throughout this area in the vicinity of the tumor. F: View of a deeper cortical area from panel B. A cross-section of a microvessel containing erythrocytes is evident, indicative of functional blood flow. The neuronal nuclei and the fibrous tissue display normal morphological characteristics. *Ctx* = cortex; *n* = necrotic area. Immunohistochemical staining for endostatin (A, C, and D) and H & E (B, E, and F), original magnification × 40 (A and B), × 200 (E), and × 400 (C, D, and F).

(Fig. 4A and B). In tumors that endogenously released murine endostatin, the microvessel density counts were reduced by 84% and the vascular area fraction was lowered by 75% compared with control tumors (for both parameters $p < 0.0001$; Fig. 4C and D). In tumors that released human endostatin, the microvessel density was 36% lower than that in the control tumors (Fig. 4D); however, the reduction in the vascular area fraction in this group was not significant.

Evaluation of In Vivo Endostatin Distribution and Tissue Toxicity

Paraffin-embedded brain sections from the treatment and control groups were immunostained to evaluate the tissue expression of endostatin. Positive staining was observed in both treatment groups (Fig. 5A), whereas no staining was observed in tumors from the control group or in normal brain tissue of animals from either the treatment or control groups (Fig. 5C). Endostatin was markedly overexpressed in the central areas of the tumors, with less expression in peripheral areas (Fig. 5A). No staining was observed in vascular endothelial cells in the tumor or in brain tissue. Endostatin was found to be uniformly distributed in the cytoplasm of the transduced BT4C cells (Fig. 5D).

Hematoxylin and eosin–stained sections were evaluated for signs of potential brain tissue toxicity, which might have

been caused by soluble endostatin produced by the tumor. Brain tissue areas adjacent to necrotic tumors displayed normal histological characteristics (Fig. 5B and E). The neuronal nuclei and the fiber networks were intact. No histopathological changes were observed in the brain vasculature in the vicinity of the tumor. The blood vessels displayed normal morphological characteristics and contained erythrocytes indicative of functional blood flow (Fig. 5F).

Discussion

Angiogenesis has been shown to be a main control switch facilitating the progression of solid tumors from microscopic lesions to macroscopic malignancies.[19] During the preangiogenic phase of tumor development, the increasing oxygen demand of proliferating neoplastic cells triggers a hypoxic response, leading to the release of proangiogenic cytokines such as vascular endothelial growth factor and platelet-derived growth factor. In turn, these soluble factors promote endothelial cell proliferation and vascular tube formation.[7,47] When an inhibitor counteracts the angiogenic process, the neoplastic cells undergo prolonged starvation, which limits tumor growth rate. The application of angiogenesis inhibitors for cancer therapy has been well established in preclinical models and several inhibitors are now being evaluated in the clinical setting.[18]

In the present work, we demonstrate that the continuous local delivery of murine endostatin significantly prolongs the survival of rats harboring intracranial BT4C gliomas. Tumor development was abolished in 40% of the rats within this treatment group with no visible tumors on macroscopic examination after 7 months. Tumor volumes within this group were shown to be significantly smaller than those in the control group. These results are in line with experimental studies on other cancer subtypes in which endostatin suppresses tumor growth.[3–5,8,16,23,26,30,33,35,37–39,48] In contrast to previous work, however, we did not observe significantly prolonged survival or tumor volume reduction after treatment with human endostatin. The reason for this discrepancy is unclear. Because the levels of murine and human endostatin produced by the cells were shown to be similar in vitro, and because the cells were made using identical retroviral vectors, our findings suggest that species-specific differences between the endostatin protein forms may be of biological importance. Human and murine endostatin differ by 25 amino acid substitutions distributed along the whole sequence string, whereas rat and murine endostatin only differ by eight amino acids (Fig 1A). It is therefore reasonable to assume that murine endostatin has a higher affinity than human endostatin for the rat receptor expressed by the host.

Tumors that overexpressed either the murine or the human species-specific form of endostatin exhibited large necrotic areas, indicating that both endostatins counteracted tumor angiogenesis. Importantly, murine endostatin significantly reduced mean plasma volume fractions, microvessel density counts, and vascular area fractions. For all these parameters, an inhibition of more than 70% was observed compared with corresponding values in the control group. This indicates that murine endostatin was very potent at inhibiting both microvessel formation and vascular function in our experimental setting. We also report a 36% reduction in mean microvessel density in the human endostatin treatment group. The vascular area fractions were lower in human endostatin–treated tumors than in control tumors, although this difference did not reach statistical significance. From the survival analysis, it seems that within both treatment groups, two subgroups were present-one group of tumors in which endostatin inhibited tumor growth and one in which it did not. The pattern seems to corroborate the on–off nature of the angiogenic switch, in which a critical level of inhibitors versus effectors has to be reached to turn off angiogenesis.

Survival correlated inversely with MR imaging–derived estimates of tumor volume and blood plasma volume (D_0), but surprisingly not with the microvessel permeability–related parameter K_2. Thus, we can infer from the MR imaging data that neither form of endostatin can hinder hyperpermeability in persistent tumor microvessels, and that the number of functional tumor vessels might be a better surrogate response indicator than the change in their permeability. The latter is supported by findings of a previous study,[37] in which no difference in microvascular permeability was found between human endostatin–treated or control C6 gliomas when analyzed using intravital microscopy.

In histological studies involving immunostaining, endostatin was found to be expressed in vivo exclusively by the transduced BT4C cells. We did not observe specific staining for endostatin throughout the host brain tissue, although we cannot rule out that soluble endostatin secreted by BT4C ENDO cells diffused outside the tumor bed. Indeed, low levels of endostatin were present in the CSF of animals in the treatment groups. Still, we did not observe any signs of normal tissue toxicity. The host brain tissue adjacent to the tumors exhibited regular histological characteristics with intact parenchyma and functional microvessels. Necrotic areas were not observed. This is in line with previous findings suggesting that soluble endostatin only affects pathological angiogenesis and does not cause any toxicity or antivascular effects in normal tissues.[43]

We injected suspensions of endostatin-secreting or mock-infected glioma cells into the rat brain to assess the effect of endostatin on angiogenesis-dependent tumor establishment and progression. We believe this approach mimics the postoperative clinical situation, in which recurrent solid lesions arise from dispersed glioma cells after the initiation of angiogenesis. Because each implanted glioma cell in the treatment group secreted endostatin, our experimental design resembles the situation following a highly successful gene therapy regimen with complete tumor transduction—one that cannot be obtained with vector systems that are currently available. Nevertheless, it provides a reliable assessment of the biological efficacy of endostatin in vivo, and as such, estimates the potential of this inhibitor when more potent vector systems are made available.

Conclusions

We report that local treatment with both human and murine endostatin led to the development of central necroses in intracranial rat gliomas. We observed interspecies cross-reactivity between both endostatin forms and the rat receptor, demonstrating a higher biological effect when the murine form was used. Importantly, overexpression of soluble murine endostatin inhibited tumor growth and improved the

survival of animals in a syngeneic rat model without any apparent toxic effects on normal brain tissue.

Acknowledgments

We thank Dr. Bjørn R. Olsen (Department of Cell Biology, Harvard Medical School, Boston, MA) for the pCEP/Pu-AC7 plasmids, and Dr. Rupert Timpl (Max-Planck-Institut für Biochemie, Matrinsried, Germany) for the rabbit anti–endostatin serum. We also thank Drs. Karl-Henning Kalland (Department of Microbiology and Immunology, University of Bergen, Norway) and Johan Lillehaug (Department of Molecular Biology, University of Bergen) for materials and for their advice. Finally, we thank Bodil B. Hansen and Tove D. Johansen for their technical assistance.

References

1. Ausubel FM, Brent R, Kingston RE, Moore DD, Seidman JG, Smith JA, et al (eds): **Short Protocols in Molecular Biology, ed 5.** New York: John Wiley & Sons, 2002
2. Blankesteijn WM, van Gijn ME, Essers-Janssen YP, Daemen MJ, Smits JF: Beta-catenin, an inducer of uncontrolled cell proliferation and migration in malignancies, is localized in the cytoplasm of vascular endothelium during neovascularization after myocardial infarction. **Am J Pathol 157:**877–883, 2000
3. Blezinger P, Wang J, Gondo M, Quezada A, Mehrens D, French M, et al: Systemic inhibition of tumor growth and tumor metastases by intramuscular administration of the endostatin gene. **Nat Biotechnol 17:**343–348, 1999
4. Blezinger P, Yin G, Xie L, Wang J, Matar M, Bishop JS, et al: Intravenous delivery of an endostatin gene complexed in cationic lipid inhibits systemic angiogenesis and tumor growth in murine models. **Angiogenesis 3:**205–210, 1999
5. Boehm T, Folkman J, Browder T, O'Reilly MS: Antiangiogenic therapy of experimental cancer does not induce acquired drug resistance. **Nature 390:**404–407, 1997
6. Boehm T, O'Reilly MS, Keough K, Shiloach J, Shapiro R, Folkman J: Zinc-binding of endostatin is essential for its antiangiogenic activity. **Biochem Biophys Res Commun 252:**190–194, 1998
7. Brat DJ, Kaur B, Van Meir EG: Genetic modulation of hypoxia induced gene expression and angiogenesis: relevance to brain tumors. **Front Biosci 8:d100–d116, 2003**
8. Chen QR, Kumar D, Stass SA, Mixson AJ: Liposomes complexed to plasmids encoding angiostatin and endostatin inhibit breast cancer in nude mice. **Cancer Res 59:**3308–3312, 1999
9. Demuth T, Berens ME: Molecular mechanisms of glioma cell migration and invasion. **J Neurooncol 70:**217–228, 2004
10. Dhanabal M, Ramchandran R, Volk R, Stillman IE, Lombardo M, Iruela-Arispe ML, et al: Endostatin: yeast production, mutants, and antitumor effect in renal cell carcinoma. **Cancer Res 59:** 189–197, 1999
11. Dhanabal M, Ramchandran R, Waterman MJ, Lu H, Knebelmann B, Segal M, et al: Endostatin induces endothelial cell apoptosis. **J Biol Chem 274:**11721–11726, 1999
12. Dhanabal M, Volk R, Ramchandran R, Simons M, Sukhatme VP: Cloning, expression, and in vitro activity of human endostatin. **Biochem Biophys Res Commun 258:**345–352, 1999
13. Dixelius J, Cross M, Matsumoto T, Sasaki T, Timpl R, Claesson-Welsh L: Endostatin regulates endothelial cell adhesion and cytoskeletal organization. **Cancer Res 62:**1944–1947, 2002
14. Eisterer W, Jiang X, Bachelot T, Pawliuk R, Abramovich C, Leboulch P, et al: Unfulfilled promise of endostatin in a gene therapy-xenotransplant model of human acute lymphocytic leukemia. **Mol Ther 5:**352–359, 2002
15. Eriksson K, Magnusson P, Dixelius J, Claesson-Welsh L, Cross MJ: Angiostatin and endostatin inhibit endothelial cell migration in response to FGF and VEGF without interfering with specific intracellular signal transduction pathways. **FEBS Lett 536:** 19–24, 2003
16. Feldman AL, Restifo NP, Alexander HR, Bartlett DL, Hwu P, Seth P, et al: Antiangiogenic gene therapy of cancer utilizing a recombinant adenovirus to elevate systemic endostatin levels in mice. **Cancer Res 60:**1503–1506, 2000
17. Ferreras M, Felbor U, Lenhard T, Olsen BR, Delaisse J: Generation and degradation of human endostatin proteins by various proteinases. **FEBS Lett 486:**247–251, 2000
18. Folkman J: Endogenous angiogenesis inhibitors. **Apmis 112:** 496–507, 2004
19. Folkman J: Fundamental concepts of the angiogenic process. **Curr Mol Med 3:**643–651, 2003
20. Folkman J: Tumor angiogenesis: therapeutic implications. **N Engl J Med 285:**1182–1186, 1971
21. Hajitou A, Grignet C, Devy L, Berndt S, Blacher S, Deroanne CF, et al: The antitumoral effect of endostatin and angiostatin is associated with a down-regulation of vascular endothelial growth factor expression in tumor cells. **FASEB J 16:**1802–1804, 2002
22. Hanai J, Dhanabal M, Karumanchi SA, Albanese C, Waterman M, Chan B, et al: Endostatin causes G1 arrest of endothelial cells through inhibition of cyclin D1. **J Biol Chem 277:**16464–16469, 2002
23. Indraccolo S, Gola E, Rosato A, Minuzzo S, Habeler W, Tisato V, et al: Differential effects of angiostatin, endostatin and interferon-alpha(1) gene transfer on in vivo growth of human breast cancer cells. **Gene Ther 9:**867–878, 2002
24. Kim YM, Hwang S, Kim YM, Pyun BJ, Kim TY, Lee ST, et al: Endostatin blocks vascular endothelial growth factor-mediated signaling via direct interaction with KDR/Flk-1. **J Biol Chem 277:**27872–27879, 2002
25. Kim YM, Jang JW, Lee OH, Yeon J, Choi EY, Kim KW, et al: Endostatin inhibits endothelial and tumor cellular invasion by blocking the activation and catalytic activity of matrix metalloproteinase. **Cancer Res 60:**5410–5413, 2000
26. Kisker O, Becker CM, Prox D, Fannon M, D'Amato R, Flynn E, et al: Continuous administration of endostatin by intraperitoneally implanted osmotic pump improves the efficacy and potency of therapy in a mouse xenograft tumor model. **Cancer Res 61:** 7669–7674, 2001
27. Kleihues P, Cavenee WK (eds): **Pathology and Genetics of Tumours of the Nervous System.** Lyon: IARC Press, 2000
28. Koblinski JE, Ahram M, Sloane BF: Unraveling the role of proteases in cancer. **Clin Chim Acta 291:**113–135, 2000
29. Kohfeldt E, Maurer P, Vannahme C, Timpl R: Properties of the extracellular calcium binding module of the proteoglycan testican. **FEBS Lett 414:**557–561, 1997
30. Kurdow R, Boehle AS, Ruhnke M, Mendoza R, Boenicke L, Sipos B, et al: Retroviral endostatin gene transfer inhibits growth of human lung cancer in a murine orthotopic xenotransplant model. **Langenbecks Arch Surg 388:**401–405, 2003
31. Laerum OD, Rajewsky MF: Neoplastic transformation of fetal rat brain cells in culture after exposure to ethylnitrosourea in vivo. **J Natl Cancer Inst 55:**1177–1187, 1975
32. Lund EL, Spang-Thomsen M, Skovgaard-Poulsen H, Kristjansen PE: Tumor angiogenesis—a new therapeutic target in gliomas. **Acta Neurol Scand 97:**52–62, 1998
33. Oga M, Takenaga K, Sato Y, Nakajima H, Koshikawa N, Osato K, et al: Inhibition of metastatic brain tumor growth by intramuscular administration of the endostatin gene. **Int J Oncol 23:** 73–79, 2003
34. Oh SP, Kamagata Y, Muragaki Y, Timmons S, Ooshima A, Olsen BR: Isolation and sequencing of cDNAs for proteins with multiple domains of Gly-Xaa-Yaa repeats identify a distinct family of collagenous proteins. **Proc Natl Acad Sci U S A 91:**4229–4233, 1994
35. O'Reilly MS, Boehm T, Shing Y, Fukai N, Vasios G, Lane WS, et al: Endostatin: an endogenous inhibitor of angiogenesis and tumor growth. **Cell 88:**277–285, 1997

36. Pawliuk R, Bachelot T, Zurkiya O, Eriksson A, Cao Y, Leboulch P: Continuous intravascular secretion of endostatin in mice from transduced hematopoietic stem cells. **Mol Ther 5:**345–351, 2002
37. Read TA, Farhadi M, Bjerkvig R, Olsen BR, Rokstad AM, Huszthy PC, et al: Intravital microscopy reveals novel antivascular and antitumor effects of endostatin delivered locally by alginate-encapsulated cells. **Cancer Res 61:**6830–6837, 2001
38. Read TA, Sorensen DR, Mahesparan R, Enger PO, Timpl R, Olsen BR, et al: Local endostatin treatment of gliomas administered by microencapsulated producer cells. **Nat Biotechnol 19:**29–34, 2001
39. Sauter BV, Martinet O, Zhang WJ, Mandeli J, Woo SL: Adenovirus-mediated gene transfer of endostatin in vivo results in high level of transgene expression and inhibition of tumor growth and metastases. **Proc Natl Acad Sci U S A 97:**4802–4807, 2000
40. Shichiri M, Hirata Y: Antiangiogenesis signals by endostatin. **FASEB J 15:**1044–1053, 2001
41. Skovseth DK, Veuger MJ, Sorensen DR, De Angelis PM, Haraldsen G: Endostatin dramatically inhibits endothelial cell migration, vascular morphogenesis, and perivascular cell recruitment in vivo. **Blood 105:**1044–1051, 2005
42. Sorensen DR, Read TA: Delivery of endostatin in experimental cancer therapy. **Int J Exp Pathol 83:**265–274, 2002
43. Sorensen DR, Read TA, Porwol T, Olsen BR, Timpl R, Sasaki T, et al: Endostatin reduces vascularization, blood flow, and growth in a rat gliosarcoma. **Neuro-oncol 4:**1–8, 2002
44. Su MY, Jao JC, Nalcioglu O: Measurement of vascular volume fraction and blood-tissue permeability constants with a pharmacokinetic model: studies in rat muscle tumors with dynamic Gd-DTPA enhanced MRI. **Magn Reson Med 32:**714–724, 1994
45. Thorsen F, Ersland L, Nordli H, Enger PO, Huszthy PC, Lundervold A, et al: Imaging of experimental rat gliomas using a clinical MR scanner. **J Neurooncol 63:**225–231, 2003
46. Yamaguchi N, Anand-Apte B, Lee M, Sasaki T, Fukai N, Shapiro R, et al: Endostatin inhibits VEGF-induced endothelial cell migration and tumor growth independently of zinc binding. **Embo J 18:** 4414–4423, 1999
47. Yancopoulos GD, Davis S, Gale NW, Rudge JS, Wiegand SJ, Holash J: Vascular-specific growth factors and blood vessel formation. **Nature 407:**242–248, 2000
48. Yoon SS, Eto H, Lin CM, Nakamura H, Pawlik TM, Song SU, et al: Mouse endostatin inhibits the formation of lung and liver metastases. **Cancer Res 59:**6251–6256, 1999

Manuscript received January 12, 2005.
Accepted in final form September 29, 2005.
This work was supported by grants from the Norwegian Ministry of Health and the Norwegian Cancer Society.

Address reprint requests to: Peter C. Huszthy, M.Sc., Gene Therapy Program, Department of Oncology and Medical Physics, Haukeland University Hospital, N-5021 Bergen, Norway. email: Peter.Huszthy@helse-bergen.no.